

Trackerless Panoramic Optoacoustic Imaging

A First Feasibility Evaluation

Suhanyaa Nitkunanantharajah* ·
Christoph Hennersperger* · Xose Luis
Dean-Ben · Daniel Razansky · Nassir
Navab

Received: date / Accepted: date

Abstract

Purpose Optoacoustic imaging provides high spatial resolution and the possibility to image specific functional parameters, therefore positioning it as a promising modality for various applications. However, despite these advantages, the usability in today's practice is limited due to its small field of view.

Methods With this work, we aim at presenting a path toward panoramic optoacoustic tomographic imaging without requiring additional sensors or position trackers. We propose a two-step seamless stitching method for the alignment and stitching of multiple datasets within a panoramic scan. The employed workflow is thereby specifically developed on the foundations of optoacoustic imaging with respect to the image properties and respective challenges.

Results An in-vivo comparison of the presented alignment shows a mean error of $628 \pm 512 \mu\text{m}$ compared to ground truth tracking data. The presented compounding scheme integrates the physical resolution of optoacoustic data and provides improved contrast in comparison to classic 3D reconstruction.

Conclusion The proposed method can produce optoacoustic volumes with an enlarged FOV and improved quality compared to current methods in optoacoustic imaging. However, our study also shows challenges for panoramic optoacoustic. In this view, we discuss relevant properties, challenges, and opportunities and present an evaluation of the performance of the presented approach depending on the input data.

*S. Nitkunanantharajah and C. Hennersperger contributed equally to this work
Computer Aided Medical Procedures, Technical University of Munich, Germany

D. Razansky and X.L. Dean-Ben
Institute for Biological and Medical Imaging, Helmholtz Center Munich, Germany

N. Navab
Computer Aided Medical Procedures, Technical University of Munich, Germany, and Johns
Hopkins University, Baltimore, USA

Keywords Volume Stitching · Trackerless Registration · Volume Compounding · Photoacoustics · Optoacoustic Imaging

1 Introduction

Optoacoustic imaging (OI) is an emerging medical imaging modality that is suitable for acquiring both structural and functional data of the human body. Based on the photoacoustic effect, it combines the advantages of optical and ultrasound (US) imaging and generates high resolution and high contrast 3D images without the use of ionizing radiation. Its high sensitivity, tissue contrast and the possibility to enhance the contrast according to the target make OI highly versatile and well-suited for multiple clinical applications. While overall penetration depths of a few centimetres are achievable with OI, this can vary heavily depending on the imaging object, as the penetration depth is dictated by the attenuation properties of the imaged soft tissue [10]. In practice, the field of view (FOV) of a single volume is commonly limited to about 1cm^3 , which is too small for many clinical applications. Thus, the FOV limits the use of the modality in practice despite its potential benefits for diagnostic imaging.

To overcome this restriction, acquiring images of larger volumes is often enabled by integrating the optoacoustic setup within mechanically actuated or tracked systems [6]. However, an integration with common tracking systems (e.g. EM or Optical tracking) is impractical due to the limited spatial accuracy of these systems, also increasing the overall system complexity. Therefore, methods that increase the FOV of conventional optoacoustic volumes *after* the image acquisition and reconstruction would be preferred. Such methods would be able to produce volumes with large FOVs while having fewer requirements on the imaging set-up and the imaging object – ultimately leading to accurate, inexpensive and highly usable solutions.

In this regard, we present a first generally applicable method that creates 3D optoacoustic volumes with a large FOV performing a trackerless stitching of several conventional volumes without any hardware modifications on the regular imaging set-up. In view of the specific challenges with respect to a trackerless stitching, it is important to address the OI characteristics, with a non-uniform resolution across each 3D volume. Both the spatial resolution and intensity contrast distribution are the highest at the centreline of the reconstructed volume, where the the emitting laser light propagates through the tissue (see Fig. 1 left). In combination with acoustic wave propagation, this results in a decrease of both resolution and intensity contrast with increasing distance to the laser focal region as well as with increasing depth [3]. Besides that, optoacoustic data exerts a high level of noise, and especially OI tomography suffers from ring-like noise structures around the focus point of the laser (see Fig. 1a). The presented approach is performed as a purely software-based pipeline and combines multiple volumes with the goal of preserving the image quality and information content of the data. By addressing some key challenges and limitations of registration-based stitching for OI, this work not

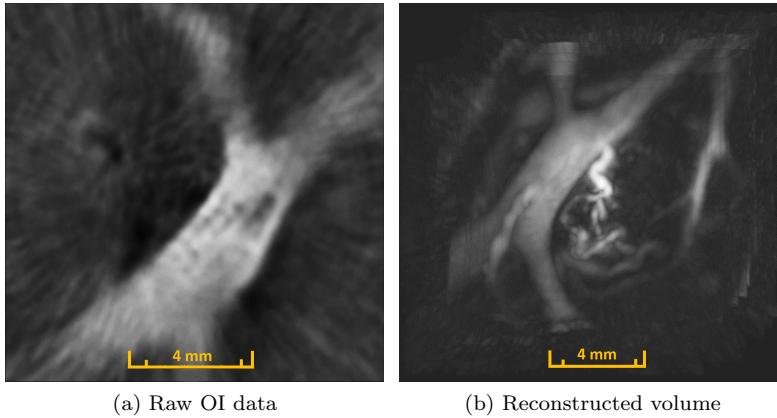


Fig. 1: 2D slice of input OI data showing the vasculature of a human wrist with characteristic ring-like noise and variation of image resolution and decreasing contrast. A MIP-projection of the reconstructed volume shows an enlarged FOV with low presence of noise.

only presents the first approach for seamless optoacoustic image-alignment and domain-specific compounding, but also aims at discussing relevant challenges and opportunities for the community.

2 Related Work

Prior work concerning the problem of the limited FOV in optoacoustic imaging usually attempted to increase the volumetric coverage in early stages of imaging, such as during the data acquisition and image formation. Kruger et al. [9] present a breast mammography system that can image larger regions by using a highly dedicated imaging setup with a specific acquisition pattern and geometry of the imaging objects. While the system can image up to a penetration depth of 53 mm, only a spatial resolution of 0.43 mm can be achieved with this imaging system. Other systems, such as the whole-body optoacoustic scanner for small animals [5] combine a dedicated imaging setup with a modified reconstruction process to enlarge the FOV. Even though this system succeeds in creating increased FOV images, the spatial resolutions is again limited to about 0.5 mm. Additionally only objects of certain sizes and shapes can be imaged, which makes this specific system not applicable e.g. for human use. A more general approach that does not influence the initial spatial resolution was developed by Fehm et al [6]. Multiple volumes are acquired in a spiral-like pattern around the object, while the scanning positions are mechanically tracked. After reconstruction, the volumes are aligned to each other based on the tracked detector positions and added up to form a single optoacoustic volume with a large FOV, a concept similar to tracked freehand 3D

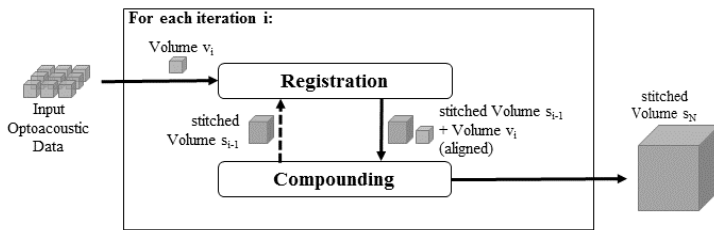


Fig. 2: Overview of the registration and reconstruction workflow.

ultrasound imaging [16]. This method is less restrictive and also applicable to different imaging set-ups, reconstruction algorithms and scanning geometries. However, it still requires some hardware modifications to track the exact scanning positions and its quality is highly dependent on the tracking accuracy.

While trackerless approaches have not yet been explored in OI, such approaches were first explored more than 10 years ago in ultrasound [12], and subsequently improved by using speckle tracking or RF signal-correlation [1]. Recently, a learning-based method for sensorless 3D-US imaging was employed in a deep-learning framework for pose estimation from a series of US images [13]. From the same group, a registration-based panoramic compounding from 3D to panoramic data was presented, employing the well-known LC2 registration similarity metric for image alignment [11]. While these results show a promising direction for trackerless compounding, the specific challenges of optoacoustic imaging impair their direct application to such datasets. This is why we discuss a tailored approach to OI data in the following.

3 Trackerless Panoramic Optoacoustic Reconstruction

The method we propose to generate 3D optoacoustic volumes with large FOVs is an iterative two-step reconstruction of multiple subvolumes with overlapping imaging regions (see Fig. 2). The input of our method is a number of OI volumes that have been acquired and tomographically reconstructed beforehand. In the first step (*registration*), the volumes are spatially aligned into the same coordinate system. In the second step (*compounding*), multiple volumes are then fused into one large volume containing all information.

The algorithm is initialized by setting the first input volume v_1 as the intermediate stitched volume s_1 . In every iteration i , the input volume v_i is then stitched with the result s_{i-1} from the previous iteration by following the steps described below.

3.1 Registration

Transformation initialization The spatial relation between the individual volumes needs to be determined computationally, as no position tracking is used.

Before the actual registration is started, an initialization can be performed to aid the process of alignment. In the beginning of the stitching, all input volumes are positioned around the origin. We presume, however, that input volumes are acquired sequentially with consecutive volumes being spatially sufficiently close with significant overlap. Therefore, at the beginning of the registration step, each input volume v_i (with $i = 2, \dots, N$ and $N =$ number of input volumes) is initialized with the position of the previous volume v_{i-1} after its alignment in order to help the registration process to converge in a short time. Once initialized, registration of the volumes is performed using a feature-map based registration approach.

Feature-based registration Most applications for OI are performed on in-vivo tissue with a high amount of vasculature, therefore vessels or vessel-like structures will exist in each volume. Taking advantage of this assumption, these structures are suited well for a coarse registration. In this view, tubular structures are extracted from each volume using the vesselness filter developed by Frangi et al. [7] based on the 3D multi-scale line filter for curvilinear structures introduced by Sato et al [14]. Tubular structures are extracted at multiple scales and the filter responses are then combined, while the noise level at each scale is estimated and equalized. Once the vessel-like structures are extracted, we estimate the centreline of the vessels to retrieve the skeleton of the vasculature visible in the image. For that, basic morphological algorithm of binary object thinning are employed to the vesselness data [8]. The extracted centrelines are then converted into a point cloud, and registered using the iterative closest point algorithm (ICP) [4]. The overall transformation calculated by ICP represents the spatial relation between the two volumes. A preliminary coarse alignment is performed using ICP and centerlines, which is sufficient for applications that do not highlight high (tissue) contrast in the OI data but prominent features such as vessels. Thus, this provides both a robust and accurate alignment, providing a fast way for registration. For applications that do not highlight vessels, other features can be determined for this initial step.

Registration refinement The initial alignment is then refined with an intensity-based registration approach. When comparing two optoacoustic volumes even with a small translational offset, we experienced in overall low similarities with metrics such as Sum of Squared Differences (SSD), Normalized Cross Correlation (NCC), or Linear Correlation of Linear Combination (LC^2) applied to the OI volumes after the feature-based alignment. While this is subject to ongoing research, we suspect the high noise level and different intensity ranges caused by laser fluctuations and other hardly controllable effects to play a role in this. As a consequence, the features maps extracted from the original image data (in our case the vesselness maps) are employed also for the intensity-based refinement. For this fine registration alignment, we use NCC as similarity metric and regular step gradient descent as optimizer.

Once the final spatial relation between the volumes is computed, it is applied to the moving volume. As a result, two aligned 3D optoacoustic volumes are retrieved, in which anatomical structures visible in both refer to the same position in space.

3.2 Compounding

In the compounding step, multiple volumes are condensed into one volume. The voxel value at each position of the output volume is computed based on the intensity values of each input volume at that position. The quality of the compounding is determined by the method used to compute the output voxel values of the volume.

While a variety of methods can be used for reconstruction, only simple operations such as addition or averaging were employed in OI so far. To achieve the goal of seamlessly stitched optoacoustic volumes with a high image quality, however, we propose compounding by inverse centre distance weighting (ICDW). Optoacoustic volumes have a non-uniform resolution throughout the volume with the highest resolution around the centreline of the volume (line of laser emission). Samples close to the centre of each OI volume provide higher resolution and thus should have a higher impact on the compounded volume than samples in regions of lower resolution with more blurry content. Taking this into account, an adapted version of Shepard’s inverse distance weighting algorithm [15] is introduced. A similar method was proposed earlier by Barry et al. [2] for 3D ultrasound compounding. Barry et al. consider the distance between a voxel and neighboring pixels in order to determine the intensity weighting. In contrast, our method computes weights based on the distance between a voxel and its volume centre point, as we approximate the area around this point to have the highest contrast and resolution.

For each voxel in the compounded volume s , each voxel in every input volume v_i (with $i = 1, \dots, N$ and $N =$ number of input volumes) mapping to the same position is weighted, summed up and normalized by the sum of all weights.

$$s(x, y, z) = \begin{cases} \frac{\sum_i^N w_i(x, y, z) \times v_i(x, y, z)}{\sum_i^N w_i(x, y, z)} & \text{if } \forall i : d_i(xyz) \neq 0 \\ v_i(x, y, z) & \text{if } \exists i : d_i(xyz) = 0 \end{cases} \text{ with } w_i = \frac{1}{d_i(x, y, z)^u} \quad (1)$$

The weights w_i for each voxel depend on the distance d_i of that voxel to the centre point of volume v_i . The further away a voxel is from its volume centre, the lower is its weight. Since the resolution drops very quickly when moving away from the centreline of the volume, u , the exponent to the distance in the weight computation, is chosen empirically to be 1 to keep the influence of outer voxel low.

4 Experiments

4.1 Experimental Setup

To test the proposed trackerless stitching method, two in-vivo acquisitions from the forearm of a healthy volunteer are acquired with 441 volumes per acquisition. The experimental set-up consists of a laser light source ($f_s = 50$ Hz), a

custom-made spherical array probe and a parallel acquisition system as well as a workstation. The object of interest is placed in a container filled with water to ensure proper acoustic coupling. The probe (**TODO: specs on frame-rate, pixel size, element count, maybe paper reference available?**) is moved over the object without immediate contact to prevent tissue distortion due to any pressure applied by the probe. For an accurate positioning and a steady and controlled movement of the probe over the imaging object, the probe is mounted on motorized linear stages (**TODO: vendor of linear stages, guaranteed accuracy"?**) that provide three degrees of freedom. On this foundation, a target area of interest can be imaged in a regular grid by moving the probe in both x and y -direction by a fixed step size τ , while the object of study remains static. Thus, the relative position of each recorded volume is known and can be regarded as ground truth alignment for the registration. Following this procedures, 21×21 volumes were acquired in a grid with isotropic step sizes of $\tau = 2.0 \text{ mm}$ between each subvolume for both acquisitions.

The acquired signals were deconvolved with the impulse response of the transducer and band-pass filtered with the cutoff frequencies of 0.1 and 8 MHz. A 3D backprojection of the filtered signals yields tomographic 3D optoacoustic images. The scans were taken at a frequency of 25 Hz and wavelength of 800 nm. The reconstructed volumes have a size of $120 \times 120 \times 200$ voxels with a resolution of $100 \frac{\mu\text{m}}{\text{vox}}$. To reduce the noise level and imaging artefacts, a fixed number of 5 frames at each position are averaged into a single volume.

The results of the stitching method were evaluated by comparing them to their reference volumes computed by adding up all input volumes after manually aligning them based on their relative positions retrieved from linear stage tracking, representing the stitching method used in related work in OI [6]. This ground truth volume is used to compare the overall performance of the proposed method with the state-of-the-art.

Additionally, a qualitative evaluation was conducted using the same data set, imaging system, and acquisition procedure, with the probe being freely operated by hand, without using the mechanical stage. However, no ground truth was available, as a comparison with conventional EM or optical tracking systems would have been likely to fail since these systems typically yield a significant reconstruction inaccuracy.

4.2 Registration Accuracy

First, a series of subvolumes for the two acquisitions outlined above is evaluated. Quantitative results are indicated in Table 1 for the offsets of the retrieved registration data compared to ground truth tracking data. It can be seen that the quality of the registration highly depends on the selected indicative input volumes. While for some volumes precise alignments can be calculated, for others the computed transformations deviate strongly from the actual alignment due to poor image quality, large variations in the intensity ranges, absence of good features for the coarse registration, multiple alignment

possibilities or too small volume overlaps. The average euclidean distance between the computed voxel positions and the positions given by the tracking is $628 \mu\text{m} \pm 512 \mu\text{m}$, with a maximum distance of $1268 \mu\text{m}$. The individual in-

Table 1: Registration offsets with mean \pm std in each direction (tx,ty,tz) and Euclidean distance d. Values are given in vox with spacing of $100 \frac{\mu\text{m}}{\text{vox}}$.

Vol.	Acquisition 1				Acquisition 2			
	tx	ty	tz	d	tx	ty	tz	d
1 (ref)	0	0	0	0	0	0	0	0
2	0.50	5.44	1.87	5.77	0.36	4.10	1.96	4.56
3	0.88	12.09	3.72	12.68	1.62	0.85	0.83	2.01
4	0.43	11.18	4.26	11.97	19.03	1.79	0.45	19.12
5	1.20	4.87	0.01	5.02	36.66	9.97	1.62	38.02
6	1.55	1.47	0.71	2.25	59.27	16.50	0.76	61.53
mean	0.76	5.84	1.76	6.28	19.49	5.53	0.94	20.87
std	0.56	4.94	1.86	5.12	24.26	6.46	0.73	24.53

put volumes for acquisition 1 contain clearly visible anatomical structures and have similar intensity ranges. Figure 3 top shows the result of the registration fused by (a) simple addition of all aligned input volumes in comparison with the (b) reference volume stitched based on the alignment given by the position tracking of the probe.

While the offset between the computed and tracked positions might appear large, the visual alignment of the proposed method outperforms the alignment given by the tracked positions due to the tracking inaccuracies and due to untracked patient motion during image acquisition.

In contrast, however, the second acquisition show partial misalignment. This is potentially caused by the input volumes for the second acquisition, having different intensity ranges with multiple anatomical structure. The visual comparison of the registration result with its corresponding reference volume (see Fig. 3 bottom) shows these errors. The alignment of the first three volumes containing various anatomical structures and strong features works with high precision. The registration of the volumes containing only a few and mainly parallel tubular structures, however, fails. For these volumes, multiple different alignments maximise the similarity function. For this reason, both coarse and fine registration fail to align those volumes properly. The average distance between the computed voxel positions and the tracked positions is $2087 \mu\text{m} \pm 2453 \mu\text{m}$, with a maximum distance of $6153 \mu\text{m}$.

These examples illustrate that the proposed registration method can produce high precision alignments, even exceeding the performance of the currently used method with position tracking. However, if a few volumes cannot be aligned sufficiently accurate, following registrations will fail as well. In this view and in reference to challenges outlined above, the proposed method can

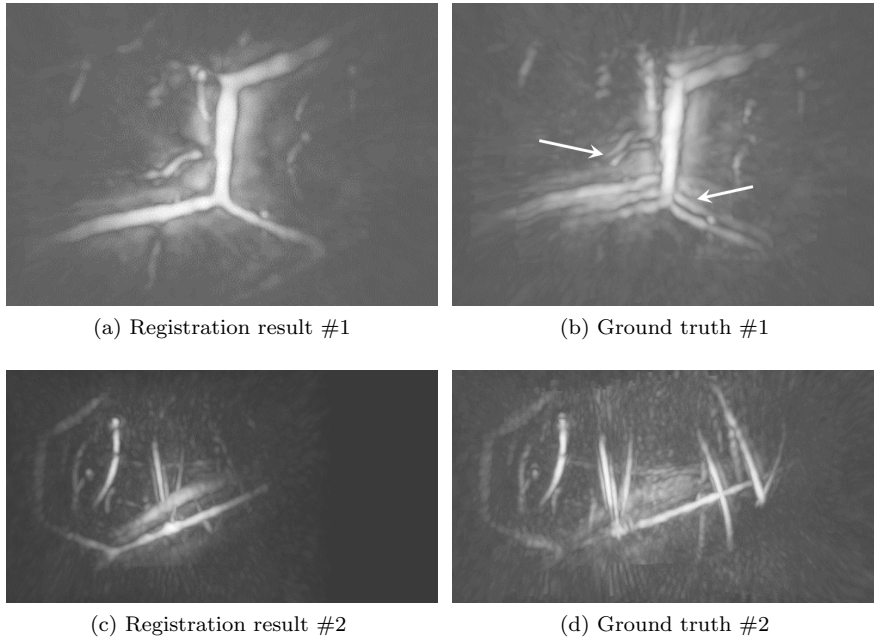


Fig. 3: Acquisition 1 (top) and acquisition 2 (bottom) - Registration outcome in comparison with reference volume (both fused by addition). Arrows indicate visible misalignment in tracked acquisition 1.

not reliably produce high accuracy alignments for all types of optoacoustic input data. Possible ways to overcome this will be discussed in Sec. 5.

4.3 Compounding Quality

The quality of the proposed compounding is assessed by aligning the volumes using the tracked position information and compounding them using the proposed ICDW method in comparison to the commonly used methods addition and averaging. The compounding quality is analyzed by stitching 100 input volumes using the three different compounding methods and comparing selected regions of interest (ROI) in the stitched results with each other. The comparison of the ROIs is found in Figure 4, indicated for a selection of representative areas within the overall volume.

Visually, the simple addition of the volumes yields images with the least overall noise and with high contrast edges (yellow ROI in Fig. 4), especially in regions where multiple volumes overlap. At the same time, the contrast and the intensity resolution decrease rapidly and anatomical structures become hardly visible (red ROI in Fig. 4). The overall image does not contain any visible seams or artefacts at stitched regions. Similar to the addition, aver-

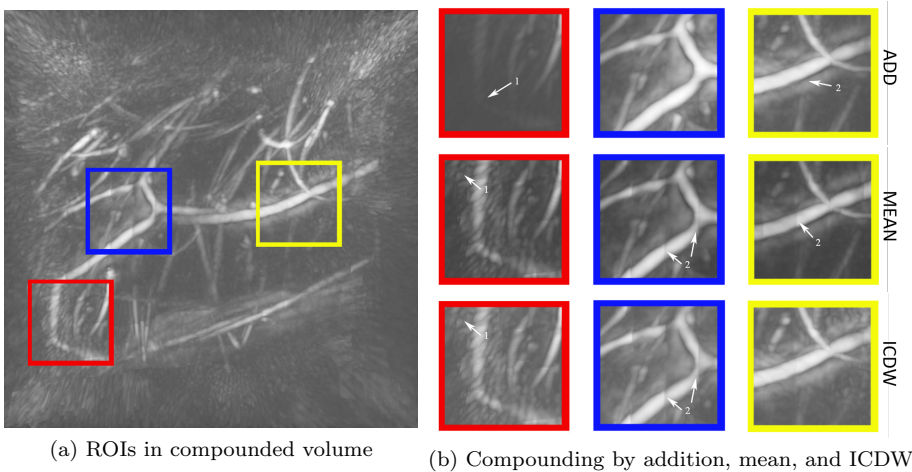


Fig. 4: Comparison of image quality for different compounding methods in selected ROIs. The arrows indicate vanishing contrast and increased noise in outer regions (1) as well as seams (2).

Table 2: Distribution of the PSNR over the whole input volumes and over the central 10 % of each input volume for different compounding methods.

	add	avg	ICDW
complete volume	13.13 ± 3.67	33.81 ± 1.96	33.69 ± 2.00
centre region	0.66 ± 3.37	17.85 ± 1.46	17.73 ± 1.70

aging also produces volumes with a low noise level in regions where multiple volumes map to. However, the fewer volumes contribute to a certain area, the more the noise becomes visible (red ROI in Fig. 4). Vessels are not as bright as in the added volume but remain with nearly the same brightness as in the input volumes. On bright structures, especially vessels, seams become slightly visible in transitional areas where the overlapping volumes change (blue and yellow ROI in Fig. 4). The volume resulting from the proposed ICDW compounding method delivers similar results to the averaging, but provides higher visual contrast and less seams. The noise level in regions where multiple input volumes map to is low and increases with decreasing number of volumes contributing to a certain area (red ROI in Fig. 4). Nevertheless, the overall noise level is slightly lower. Static structures, especially vessels, have a high contrast and a brightness similar to the input volumes. Vessel edges appear slightly sharper compared to add compounding.

For a quantitative assessment of the compounding, the peak signal-to-noise-ratio (PSNR) between each OI input volume and its corresponding region in the stitched volume is computed for the three compounding methods (see Table 2). Due to the non-uniform image quality within an input OI volume,

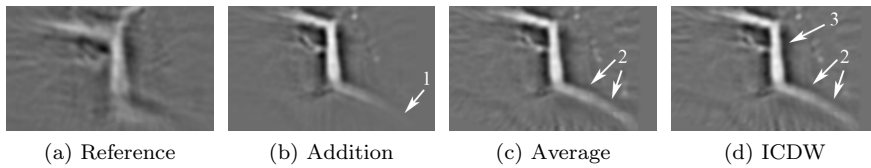


Fig. 5: Results of seamless stitching in comparison to reference volume, using adding, averaging, or ICDW compounding. Arrows indicate vanishing contrast for anatomical structures (1), slightly visible seams (2), and sharper edges (3).

with the highest image quality at the central region of each volume (see Fig. 1), we evaluate the PSNR for both full volume and centre regions, respectively. It can be observed that the distribution of the PSNRs is similar for both averaging and ICDW compounding, while it is significantly lower for volumes fused by addition, as addition enlarges the intensity range in the resulting volume, while the other methods select values within the original intensity range.

Taking the results of both the qualitative and the quantitative analysis into account, both averaging and ICDW compounding preserve a similar amount of information. ICDW compounding, however, produces volumes with slightly sharper edges and less noise than mean compounding, while being less sensitive to intensity range variations in the input data and, therefore, producing less seams (See Fig. 4).

4.4 Overall Stitching Performance

The performance of the overall stitching method is evaluated by comparing the volumes stitched by the proposed method with the reference volume as well as with volumes registered as proposed and compounded with addition or averaging. The alignment using the proposed registration method performs better than the alignment using the probe position tracking. However, comparing the outcome of the registration step, slight variations in the computed alignments can be noticed depending on the chosen compounding method. Visually, the overall stitched volumes (see Fig. 5) provide similar results as described in the previous sections. Averaging and ICDW compounding produce good results, exceeding the quality of the volumes fused with addition. The ICDW compounding, however, depicts fine structures with increased sharpness compared to the averaging.

Applying the proposed method on the data acquired with the free-hand acquisition system shows similar results (Figure 6). As this data was acquired without position tracking, no reference alignment is available. Nevertheless, visually, the computed alignments appear accurate and the registration delivers very similar results independent of the chosen compounding method. Especially for the fine bright structures in the central region of the volume,

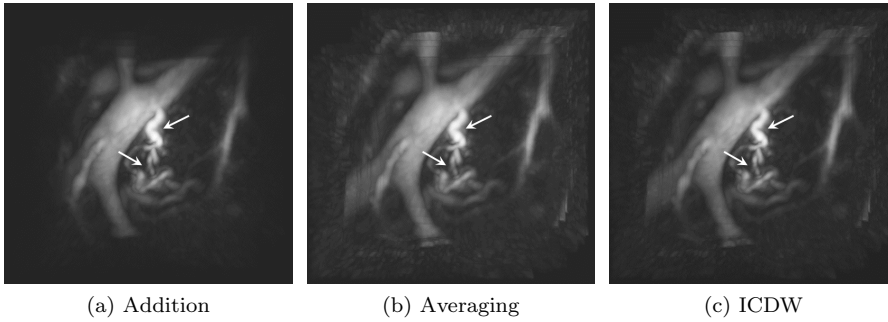


Fig. 6: Results for free-hand guidance using different compounding method. Arrows are indicating differences in fine structure contrast.

the quality of the ICDW compounding can be seen in comparison to addition or averaging as compounding method.

5 Discussion and Conclusion

Based on the results presented above, the overall trackerless method succeeds in enlarging the FOV of optoacoustic images for whereas the quality of the outcome depends on the quality of the input volumes and the chosen compounding method. The selected type of compounding influences the alignment of the volumes. Although averaging can produce good results, ICDW is the preferred compounding method as it regards for the properties of the raw OI volumes, and thus performs slightly better in preserving the high resolution of the volumes and is less sensitive to variations in the image quality and especially in the intensity ranges. To further improve the quality of the final reconstructions, additional preprocessing of the OI data could be employed, where a normalization of the intensity distribution could be employed as well as a removal of ring-like artefacts.

With respect to the resulting quality of the panoramic scans, however, the compounding method shows a significantly lower impact than the registration error. Our results show that for a high overlap between individual OI volumes as well as for a high image quality of the raw data, the feature-based registration can allow for convincing results. However, feature-based registration still requires a significant overlap between volumes. In our case, an offset of approximately 17% for subsequent volumes led to mis-registrations in combination with the partially low image quality. Interestingly, we achieved better results for the data acquired in free-hand guiding mode, where a higher acquisition rate of the OI system resulted in a lower offset between subsequent volumes. Further challenges in OI to be dealt with by the research community are potential occlusions in the sensitive image data, as well as potential deformation artefacts caused by pressure applied to the skin while scanning. One

way to overcome the partial misalignment of volumes would be a detection and rejection by evaluating the similarities and match of registered structures. In this view, it would be also interesting to explore a sequential algorithm structure, where each volume is registered to all other volumes to determine accurate alignment. Finally, simple sensor concepts (e.g. gyroscopic tracking) could be used as auxiliary way to augment the tracking data, thus increasing the robustness of registration-based approaches.

To this end, the method presented in this work can produce high quality results, but represents only a first step towards reliable 3D-panoramic optoacoustic imaging. We see this area as promising direction for further research, ultimately leading to a stronger presence of optoacoustic imaging in various clinical areas. By decreasing the system complexity and removing requirements with respect to acquisition protocols, trackerless panoramic OI could help to impact the lives of patients in a positive way.

References

1. Afsham, N., Rasoulia, A., Najafi, M., Abolmaesumi, P., Rohling, R.: Nonlocal means filter-based speckle tracking. *IEEE Transactions on Ultrasonics, Ferroelectrics, and Frequency Control* **62**(8), 1501–1515 (2015)
2. Barry, C., Allott, C., John, N., Mellor, P., Arundel, P., Thomson, D., Waterton, J.: Three-dimensional freehand ultrasound: image reconstruction and volume analysis. *Ultrasound in Medicine & Biology* **23**(8) (1997)
3. Beard, P.: Biomedical photoacoustic imaging. *Interface focus* (2011)
4. Besl, P.J., McKay, N.D., et al.: A method for registration of 3-D shapes. *IEEE Transactions on Pattern Analysis and Machine Intelligence* **14**(2) (1992)
5. Brecht, H.P., Su, R., Fronheiser, M., Ermilov, S.A., Conjusteau, A., Oraevsky, A.A.: Whole-body three-dimensional optoacoustic tomography system for small animals. *Journal of Biomedical Optics* **14**(6) (2009)
6. Fehm, T.F., Deán-Ben, X.L., Ford, S.J., Razansky, D.: In vivo whole-body optoacoustic scanner with real-time volumetric imaging capacity. *Optica* **3**(11) (2016)
7. Frangi, A.F., Niessen, W.J., Vincken, K.L., Viergever, M.A.: Multiscale vessel enhancement filtering. In: *International Conference on Medical Image Computing and Computer-Assisted Intervention* (1998)
8. Gonzalez, R.C., Woods, R.E.: *Digital Image Processing* (3rd Edition). Prentice-Hall, Inc. (2006)
9. Kruger, R.A., Kuzmiak, C.M., Lam, R.B., Reinecke, D.R., Del Rio, S.P., Steed, D.: Dedicated 3D photoacoustic breast imaging. *Medical physics* **40**(11) (2013)
10. Lutzweiler, C., Razansky, D.: Optoacoustic imaging and tomography: reconstruction approaches and outstanding challenges in image performance and quantification. *Sensors* **13**(6) (2013)
11. Müller, M., Helljesen, L.E.S., Prevost, R., Viola, I., Nylund, K., Gilja, O.H., Navab, N., Wein, W.: Deriving anatomical context from 4D ultrasound. In: *VCBM*, pp. 173–180 (2014)
12. Prager, R.W., Gee, A.H., Treece, G.M., Cash, C.J., Berman, L.H.: Sensorless freehand 3-d ultrasound using regression of the echo intensity. *Ultrasound in Medicine & Biology* **29**(3), 437–446 (2003)
13. Prevost, R., Salehi, M., Sprung, J., Bauer, R., Wein, W.: Deep learning for sensorless 3D freehand ultrasound imaging. In: *International Conference on Medical Image Computing and Computer-Assisted Intervention*, pp. 628–636. Springer (2017)
14. Sato, Y., Nakajima, S., Atsumi, H., Koller, T., Gerig, G., Yoshida, S., Kikinis, R.: 3D multi-scale line filter for segmentation and visualization of curvilinear structures in medical images. In: *CVRMed-MRCAS'97* (1997)

15. Shepard, D.: A two-dimensional interpolation function for irregularly-spaced data. In: Proceedings of the 1968 23rd ACM national conference. ACM (1968)
16. Solberg, O.V., Lindseth, F., Torp, H., Blake, R.E., Hernes, T.A.N.: Freehand 3D ultrasound reconstruction algorithms – a review. *Ultrasound in Medicine & Biology* **33**(7), 991–1009 (2007)